Photonic Quantum State Tomography Using Free Electrons

Alexey Gorlach,[1] Salomon Malka,[1] Aviv Karnieli,[2] Raphael Dahan,[1] Eliahu Cohen,[3] Avi Pe'er,[4] and Ido Kaminer[1,*]

[1]Solid State Institute, Technion-Israel Institute of Technology, Haifa 32000, Israel
[2]Department of Applied Physics, Stanford University, Stanford, California 94305, USA
[3]Faculty of Engineering and the Institute of Nanotechnology and Advanced Materials, Bar-Ilan University, 52900 Ramat-Gan, Israel
[4]Department of Physics and the Institute of Nanotechnology and Advanced Materials, Bar-Ilan University, 52900 Ramat-Gan, Israel

(Received 21 June 2024; accepted 18 November 2024; published 20 December 2024)

The tomography of photonic quantum states is key in quantum optics, impacting quantum sensing, computing, and communication. Conventional detectors are limited in their temporal and spatial resolution, hampering high-rate quantum communication and local addressing of photonic circuits. Here, we propose to utilize free electron-photon interactions for quantum state tomography, introducing electron homodyne detection with potential for femtosecond-temporal and nanometer-spatial resolutions. The detectable quantum information level depends on the electron-photon interaction strength. Our Letter opens avenues for free-electron-based photodetection utilizing the ultrafast, subwavelength, nondestructive nature of free electrons.

DOI: 10.1103/PhysRevLett.133.250801

Introduction—Advances in quantum optics [1–4] over the past decades enabled fundamental tests of quantum mechanics [5,6], measurement of the quantum photonic states [7–9], and the realization of quantum technologies [10–14]. These achievements stem from the development of photon detection schemes like the Hanbury Brown-Twiss experiment [15], coincidence measurements [6], photon-number resolving detectors [16,17], and homodyne detection [7–9] for quantum state tomography [18–20]. Conventional quantum-optical detectors rely on the interaction of photons with solid-state systems such as avalanche photodiodes [21–23], superconducting nanowires [24,25], and photomultiplier tubes [26,27]. Other sensitive quantum optical detectors rely on photonic interactions with effective two-level systems (e.g., atoms, trapped ions, or superconducting qubits) [28–32]. More advanced detection schemes facilitate optical nonlinearities to increase the detection bandwidth [33,34]. However, current quantum-optical techniques are limited in spatial resolution and have restricted detection rates and bandwidths due to the response time of electronic components.

Here, we propose a quantum-optical detection scheme using free electron-photon entanglement [35–37] for quantum photonic state tomography. We show how a homodyne-type free-electron interaction with a photonic state (Fig. 1) extracts the maximal information about this state in phase space via electron energy spectra measurements. This approach, which we call free-electron quantum-optical detection (FEQOD), has a fundamental information limit set by the electron-photon coupling strength, allowing quantum photonic state and Wigner function reconstruction only for sufficiently strong coupling.

Recent experiments have shown increasing electron-photon coupling constants g_q [38–41,43–46], toward the strong coupling $|g_q| \sim 1$ required for quantum state reconstruction, which was theoretically explored [47–50] and experimentally observed [51]. Additionally, classical homodyne-type detection [52–54] and sensitivity to photon statistics [55] have been demonstrated using free electrons. Altogether, unlike conventional detectors, FEQOD offers femtosecond temporal resolution due to the ultrafast PINEM interactions [38,40,41,43–46,52–56] and can achieve nanometer spatial resolution due to the small de Broglie electron wavelength in electron microscopes. This combination of high resolution across temporal and spatial domains makes FEQOD promising for applications requiring local addressing and selectivity among multiple spectral modes [57] at high modulation rates [58], particularly in photonic chips [59,60] for quantum information processing.

Extracting quantum information from electron-photon interaction—Recent interest in free-electron quantum optics spawned from theoretical and experimental advances in photon-induced nearfield electron microscopy (PINEM) [35,38–46,50,52–56,61,62], which showed how free-electron wavepackets can coherently absorb and emit multiple photons. The free electron-photon interaction strength is maximized when phase-matching conditions are met [38], allowing the electron to selectively interact with individual photonic modes to extract their quantum state [45] or interact with several modes simultaneously to extract the quantum state of a propagating photonic wavepacket.

FEQOD relies on the interaction between free electrons and photons. Here, we investigate how much information

*Contact author: kaminer@technion.ac.il

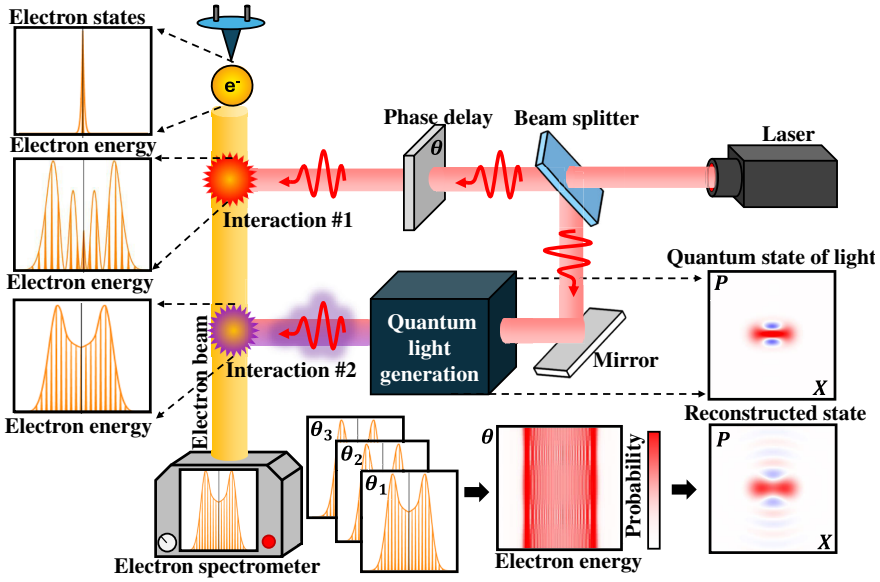

FIG. 1. Free-electron quantum-optical detection (FEQOD). Center right: FEQOD scheme. A free electron interacts with a coherent state acting as a local oscillator (interaction #1), having the same frequency and phase-locked with the target quantum signal (interaction #2). The photonic structure should support a mode with a strong electric field component parallel to the electron velocity, yielding a high value when integrated along the electron trajectory. This mode's phase velocity should match the electron velocity, fulfilling the phase-matching condition [38]. Potential experimental implementations include metal tips [35,39], photonic crystals [40], whispering gallery modes in microspheres [41], Cherenkov phase-matched structures [38], silicon-photonic dielectric laser accelerators [42], and integrated silicon photonic waveguides [43–45]. Bottom: postinteracted electrons are measured by electron energy-loss spectroscopy. Scanning the phase θ between the coherent reference and the target photonic state provides multiple electron spectra, which are used for the reconstruction of the Wigner function of the quantum signal. Reconstruction accuracy improves with stronger electron-photon coupling. Left: example electron energy spectra before interactions, after interaction #1, and after interaction #2.

about the quantum photonic state is in the electron energy spectrum following such interaction. The interaction between a free electron and a single-mode photonic state is described by the scattering matrix [36,37]

$$\hat{S} = \exp\left[g_{\mathrm{q}}\hat{b}\hat{a}^{\dagger} - g_{\mathrm{q}}^{*}\hat{b}^{\dagger}\hat{a}\right], \tag{1}$$

where $\hat{a}$, $\hat{a}^{\dagger}$ and $\hat{b}$, $\hat{b}^{\dagger}$ are the energy ladder operators for the photonic state and the free electron respectively. The $\hat{b} \equiv e^{-i(\omega/v)z}$ ladder operator represents an electron losing energy $\hbar\omega$ under the paraxial and no-recoil approximations, with v being the electron velocity and z its longitudinal position operator. The commutation relation is $\left[\hat{b}, \hat{b}^{\dagger}\right] = 0$. The approximations used in Eq. (1) hold when the electron energy E_0 (around 100 keV [35]) is much larger than the photon energy (around eV in the optical domain and much lower for THz or microwave photonics).

As building blocks for the FEQOD scheme, we define comb electron states as follows:

$$|\mathrm{comb}(\phi)\rangle = \frac{1}{\sqrt{2\pi}}\sum_{k=-\infty}^{+\infty} e^{ik\phi}|E_k\rangle, \tag{2}$$

where $|E_k\rangle$ is a narrow energy state of the electron (i.e., energy uncertainty narrower than any other energy scale) with energy $E_k = E_0 + \hbar\omega k$, around the reference energy E_0. Pure comb states have infinite energy and cannot be normalized. However, they can be well-approximated by broadband superpositions of discrete electron energy states, preparable through PINEM [63]. Comb electrons form a complete orthonormal basis $\langle\mathrm{comb}(\phi)|\mathrm{comb}(\phi')\rangle = \delta(\phi - \phi')$, so that any pure state of the electron, which is a superposition of discrete energies $|E_k\rangle$, can be decomposed on this basis. Moreover, comb electrons are the eigenfunctions of the scattering matrix S from Eq. (1):

$$\hat{S}|\mathrm{comb}(\phi)\rangle = \hat{D}\left(g_{\mathrm{q}}e^{i\phi}\right)|\mathrm{comb}(\phi)\rangle, \tag{3}$$

where $D\left(g_{\mathrm{q}}e^{i\phi}\right) = \exp\left[g_{\mathrm{q}}e^{i\phi}\hat{a}^{\dagger} - g_{\mathrm{q}}^{*}e^{-i\phi}\hat{a}\right]$ is the coherent displacement operator [2]. For comb electrons, the free electron-photon interaction acts as a displacement on the photonic field without changing the electron's state (Fig. 2(a)). Thus, the comb electron stays unentangled with photons after the interaction. Since FEQOD relies on electron-photon entanglement, interaction with a comb electron state provides no information about the photonic state.

Let's investigate how the scattering matrix acts on an arbitrary electron state $|\psi_{\mathrm{e}}\rangle$, decomposed into a superposition of combs,

$$|\psi_{\mathrm{e}}\rangle = \sum_{k=-\infty}^{+\infty} a_k|E_k\rangle = \int_{-\pi}^{+\pi} c_{\phi}|\mathrm{comb}(\phi)\rangle d\phi. \tag{4}$$

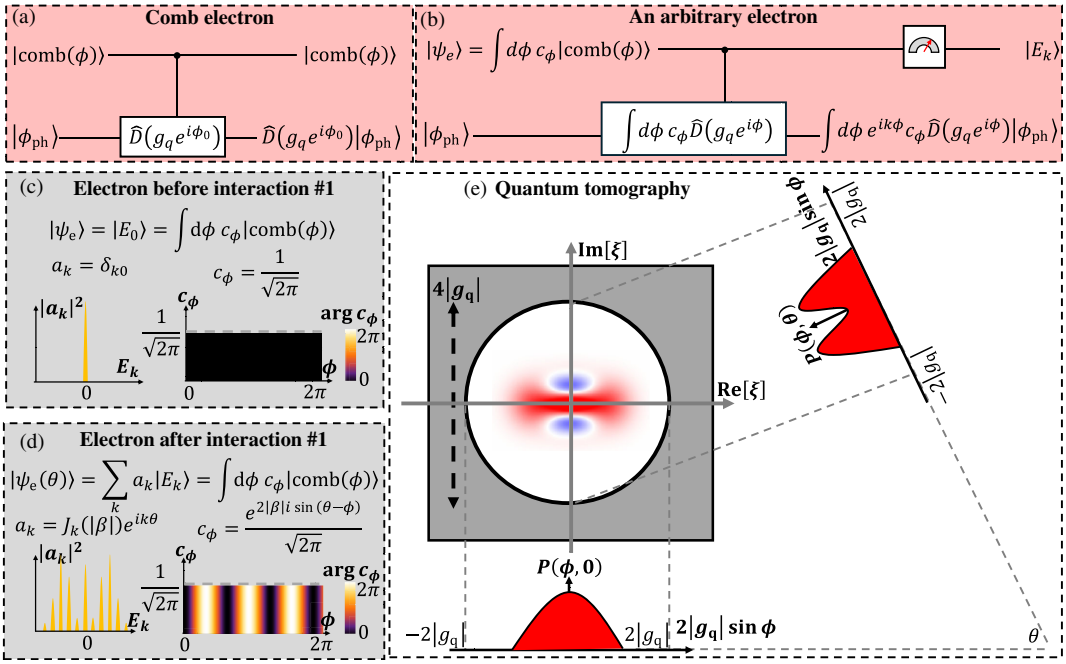

FIG. 2. Quantum-informational aspects of free electron-photon interaction. (a) A comb electron interacting with a photon state results in a displacement without altering the electron's state. Consequently, the electron spectrum after this interaction has no information about the quantum photonic state. (b) Any noncomb electron state entangles with the photons during the interaction. Measuring the electron energy spectrum in this case unveils information about the target quantum signal. (c) An initial single-energy electron $|E_0\rangle$ is a superposition of all comb electrons with equal amplitudes and phases. (d) After shaping (interaction #1) using a coherent photonic state with relative phase θ, the electron remains in a superposition of all comb states with equal amplitudes but different phases dependent on θ. (e) The quantum photonic state can be reconstructed from the Fourier series of the electron spectrum $P_k(\theta)$, which is $P(\phi,\theta)=\sum_k e^{ik\phi}P_k(\theta)$.

The coefficients a_k and c_ϕ are connected by the Fourier series relation $a_k=(2\pi)^{-1/2}\int_{-\pi}^{+\pi}c_\phi e^{ik\phi}d\phi$. Then, the action of the scattering matrix on this state is

$$\hat{S}|\psi_e\rangle=\int_{-\pi}^{+\pi}d\phi c_\phi\hat{D}\left(g_q e^{i\phi}\right)|\mathrm{comb}(\phi)\rangle. \tag{5}$$

The final state of the electron becomes entangled with the photonic state because the phase of the coherent displacement is dependent on the comb phase ϕ in Eq. (2) [see also Fig. 2(b)]. The probability of measuring electron energy E_k, i.e., the electron energy spectrum, is

$$P_k=\frac{1}{2\pi}\int_{-\pi}^{+\pi}d\phi\, e^{ik\phi}e^{i|g_q|^2\sin\phi}\times\int_{-\pi}^{+\pi}d\alpha\, c_{\phi+\alpha}c_\alpha^* C_s\left(g_q e^{i\alpha}(e^{i\phi}-1)\right), \tag{6}$$

where $C_s(\xi)=\mathrm{Tr}\left[\rho_{\mathrm{ph}}\hat{D}(\xi)\right]$ is the photonic characteristic function [4] with ρ_{ph} being the density matrix. This function describes the photonic quantum state and relates to the Wigner function: $W(\beta)=\pi^{-2}\int d^2\xi C_s(\xi)e^{\beta\xi^*-\beta^*\xi}$. According to Eq. (5), only the part of the characteristic function $\xi=g_q e^{i\alpha}(e^{i\phi}-1)$ that satisfies $|\xi|\le 2|g_q|$ contributes to the formation of the electron spectrum P_k. Consequently, P_k contains no information about the characteristic function outside the region of $|\xi|\le 2|g_q|$. This sets a limit on the information we can extract from the electron energy spectrum: the characteristic function $C_s(\xi)$ can be reconstructed only inside a circle $|\xi|\le 2|g_q|$ [Fig. 2(e)].

We formulate the FEQOD reconstruction procedure according to Eq. (6): (i) the electron is emitted with a single energy $|E_0\rangle$ [Fig. 2(c)]. The Supplemental Material (SM) [64] shows that it is impossible to reconstruct the photonic state using a single energy electron state $|E_0\rangle$. (ii) The emitted electron interacts with a reference photonic coherent state $|\alpha\rangle$ with phase $\theta=\arg\alpha$ (interaction #1). Consequently, the electron is shaped by the interaction and the phase θ is imprinted on the coefficients $c_\phi(\theta)$ [Fig. 2(d), Eq. (7)]. (iii) Then, the electron interacts with the target photonic state (labeled as interaction #2), and its energy is measured. The process is repeated for multiple electrons to get the spectrum $P_k(\theta)$, described by Eq. (6). (iv) Finally, the electron energy spectrum $P_k(\theta)$ is measured for different coherent reference phases. Using the inverse transform of $P_k(\theta)$, [4] we reconstruct $C_s(\xi)$ within the circle $|\xi|\le 2|g_q|$ [Fig. 2(e); SM].

There are several options for electron states allowing the reconstruction of $C_s(\xi)$. We consider the most experimentally accessible one, as described in step (ii), which utilizes electron shaping using a coherent photonic state of phase θ. This procedure is analogous to optical homodyne detection, where the target photonic state is superimposed with the coherent local oscillator of phase θ on a beam splitter. By varying θ, the target photonic state can be reconstructed.

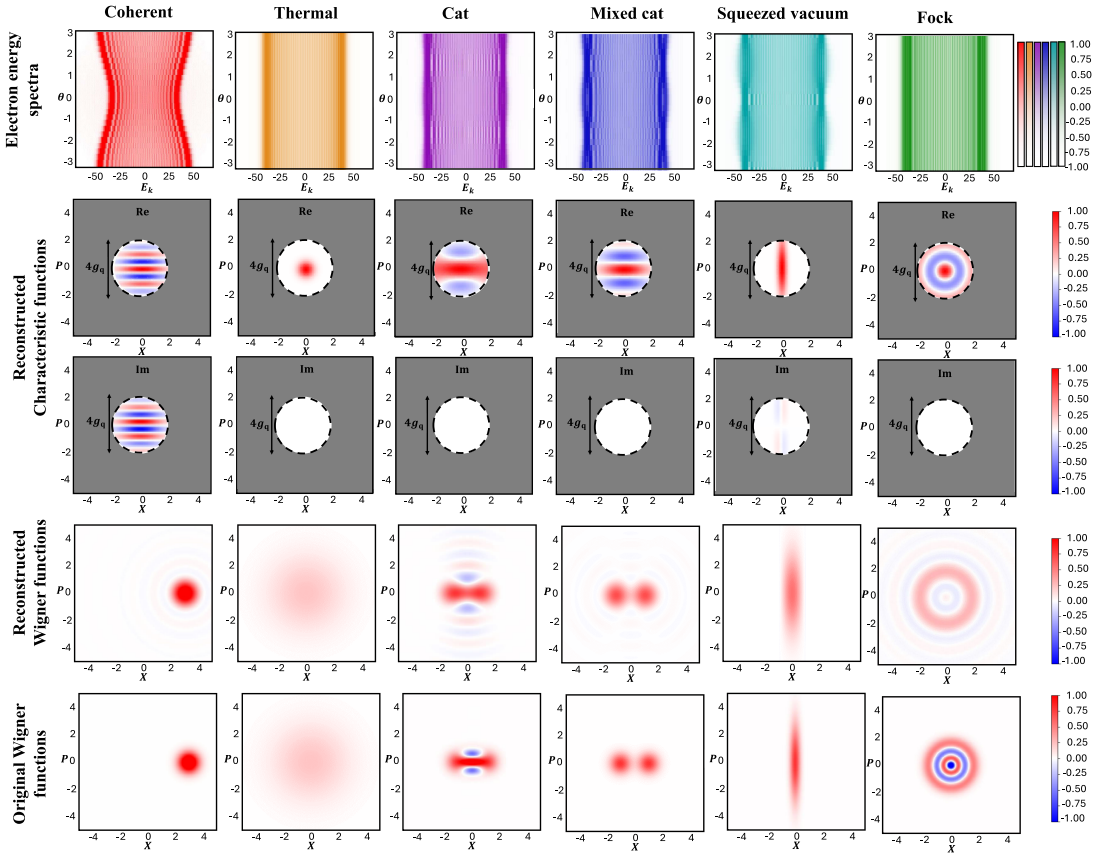

FIG. 3. Reconstruction of Wigner functions from electron energy spectra. (a) Electron energy spectra vs delays θ for coherent, thermal, cat, mixed cat, squeezed vacuum, and Fock photonic states. (b) Reconstructed real and imaginary parts of the characteristic functions according to Eq. (8) for the corresponding states. Only the part of the characteristic function inside the circle of radius $2|g_{\mathrm{q}}|$ is reconstructed, while other parts are inaccessible. (c) Reconstructed Wigner functions via Fourier transform of the reconstructed characteristic function [4]. (d) Original Wigner functions for comparison. In the simulation, the mean photon number is 3 for Fock, coherent, thermal, and squeezed vacuum states, or 1 for cat and mixed-cat states; $|\beta| = 20$ and $g_{\mathrm{q}} = 1.0$. Larger g_{q} improves reconstruction of negative Wigner function features (SM).

In our scheme, the electron wavefunction acts as the beam splitter, mediating interference between the local oscillator and the target signal.

Reconstruction of the quantum photonic state—In this section, we show that the electron wavefunction shaped by a coherent photonic state can extract maximum information about the target photonic state [Fig. 2(e)]. The relative phase between the coherent reference and the target quantum state is θ. Initially, the electron has a single energy $|E_0\rangle$ [Fig. 2(c)]. After the interaction with the local oscillator, the electron is described by [Fig. 2(d)] [61]

$$|\psi_{\mathrm{e}}(\theta)\rangle = \sum_{k=-\infty}^{+\infty} J_k(|\beta|) e^{ik\theta} |E_k\rangle = \frac{1}{\sqrt{2\pi}} \int_{-\pi}^{+\pi} d\phi e^{2|\beta| i \sin(\theta-\phi)} |\mathrm{comb}(\phi)\rangle, \quad (7)$$

where $\beta = g_{\mathrm{q}}\sqrt{\langle n\rangle}$ is the semiclassical coupling constant between the electron and a strong coherent reference with $\langle n\rangle$ average number of photons; J_k are Bessel functions of the first kind.

The comb coefficients in Eq. (5) for the spectrum are $c_\phi(\theta) = (2\pi)^{-1/2} e^{2|\beta| i \sin(\theta-\phi)}$. Electron energy spectra $P_k(\theta)$ are measured for different delays θ, enabling reconstruction of the characteristic function inside the circle of radius $2|g_{\mathrm{q}}|$ via the inverse transformation (SM),

$$C_s\left(2ig_q e^{i\alpha} \sin\frac{\phi}{2}\right) = \frac{e^{-i|g_q|^2 \sin\phi}}{\sqrt{2\pi}} \sum_n \frac{e^{-in\alpha}}{J_n(4|\beta| \sin\phi) i^n} \times \int_{-\pi}^{+\pi} d\theta e^{in\theta} \sum_k P_k(\theta) e^{-ik\phi}, \quad (8)$$

where $\alpha \in [0, 2\pi]$ and $\phi \in [0, \pi]$. This allows us to reconstruct $C_s(\xi)$ inside the circle $|\xi| < 2|g_{\mathrm{q}}|$ from the measured spectra $P_k(\theta)$. Equation (8) can be significantly simplified if $|\beta| \gg 1$ (SM). Moreover, the Fourier transform of the reconstructed characteristic function gives the Wigner function [4]. We simulated Eq. (8) for different quantum photonic states in Fig. 3.

The limitation restricting the characteristic function within a circle of radius $2|g_{\mathrm{q}}|$ sets a boundary on the precision of the quantum state reconstruction (SM). This

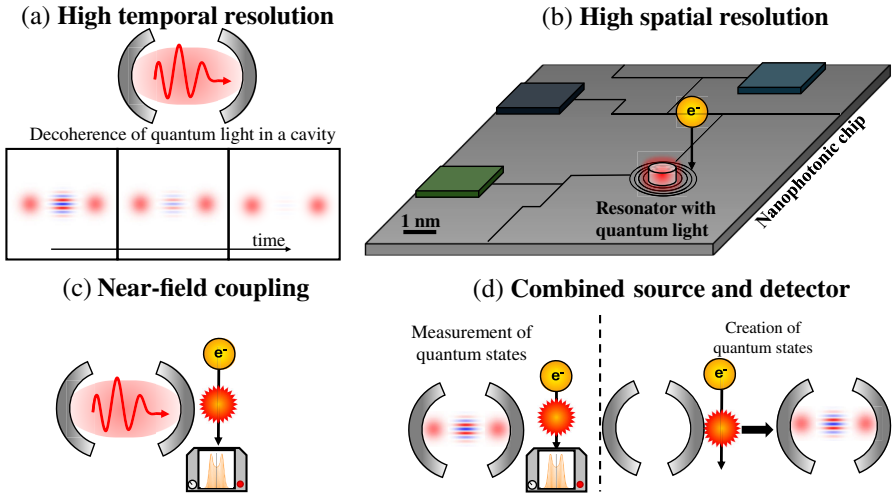

FIG. 4. Prospects of FEQOD. (a) Femtosecond temporal resolution enables tracking real-time dynamics and mapping the decoherence of quantum states. (b) Nanometer spatial resolution allows measuring quantum photonic states in nano-resonators and addressing desired points in dense optical circuits. (c) The electrons modify but do not destroy quantum photonic states during measurement, enabling in-cavity measurements without coupling photons out. (d) Free electrons can generate [71–76] and measure different photonic states in cavities, providing a complete quantum optics toolset.

boundary imposes significant limitations on the states that can be successfully reconstructed. Figure 3 presents a conservative reconstruction approach, assuming the unknown part of the characteristic function $C_s(\xi)$ with $|\xi| \geq 2|g_q|$ to be zero. This results in a reconstructed Wigner function being different from the original, as shown in Fig. 3. However, incorporating prior information about the target state can substantially improve the accuracy of the reconstructed Wigner function for the same g_q. This improvement is achieved by making informed estimates of the unknown part of the characteristic function. This highlights the importance of prior knowledge in enhancing the efficiency and accuracy of quantum state reconstruction.

Discussion—Recent PINEM advancements [38,40,41,43–46,52–56] make FEQOD promising using current laser-driven electron microscopes. Experimental demonstrations of free electron-photon interactions show an ever-increasing coupling constant g_q [38–40,43,44,46,65]. Structures for reaching the strong-interaction regime include photonic crystals [40], whispering gallery modes in microspheres [41], Cherenkov phase-matched structures [38], silicon-photonic dielectric laser accelerators [42], and integrated silicon photonic waveguides [43–45]. A coupling constant $|g_q| \sim 1$ was recently observed in a hybrid photonic-plasmonic structure [51], showing spontaneous emission of a few plasmonic quanta per electron. The recent theoretical analysis predicted promising g_q upper bounds [47,66], and nonlinearities in electron-guiding structures [50].

FEQOD is inspired by homodynelike quantum state tomography schemes proposed for cavity quantum electrodynamics with flying atoms [30,31]. Unlike two-level atomic systems, FEQOD can reconstruct the characteristic function using a single coupling constant, varying only the local oscillator phase, making it adaptable to various discrete energy level systems.

FEQOD offers several prospects in comparison to conventional quantum optical detectors, which are limited by spatial resolution, integration time, and detection rate [34,35,67]. It provides femtosecond temporal resolution [Fig. 4(a)], owing to the ultrafast PINEM interaction [38,40,41,43–46,52–56], with the potential for subfemtosecond timescales [56,68–70]. Another key advantage of FEQOD is its nanometer spatial resolution when implemented in electron microscopes [Fig. 4(b). Thus, FEQOD can visualize quantum photonic properties in time and space with deep subwavelength resolution, which is especially important for designing and validating photonic chips [59,60] for quantum information processing.

Unlike conventional quantum state tomography schemes, FEQOD can probe quantum states nondestructively, even inside cavities, resonators, and integrated nanostructures. This eliminates the need to couple photons out of the system, making it ideal for studying quantum phenomena in complex photonic circuits or nanoscale devices [Fig. 4(c)].

Another attractive feature of FEQOD is the inherent tunability of free electrons, which do not have a fixed resonance frequency. Consequently, FEQOD can be adapted to systems at different energy scales, from the optical to the microwave domains. In both domains, FEQOD enables real-time mapping of the photonic state's dynamics, e.g., following the decoherence dynamics of a Schrödinger cat state (similar to [31]). In the optical domain, FEQOD's nanometer resolution enables precise characterization of quantum photonic chips, such as measuring entangled photon states in complex on-chip interferometers or visualizing the spatiotemporal profiles of quantum photonic states inside photonic waveguides. In the microwave

domain, FEQOD could measure squeezed photonic states inside circuit quantum electrodynamics, and facilitate tomography of complex states in cavities and waveguides, e.g., reconstructing states of bosonic codes in continuous variable quantum information processing [77–79].

These features position FEQOD as a powerful tool for quantum optics research, offering insights not readily accessible through other approaches. This Letter contributes to free-electron quantum optics and adds quantum state tomography to analytical electron microscopy [35,38–46,50,52–56,61,62] and spectroscopy [80] toolboxes. Recent suggestions to use electrons to generate and control quantum photonic states [71–76] broaden the applications of FEQOD to measure these photonic states without additional optical detectors [Fig. 4(d)]. The FEQOD concept can potentially apply to other quantum information processing platforms, such as superconducting qubits [81], neutral atoms [82], and free-electron bound-electron interaction [83–88].

The implementation of FEQOD faces several technical challenges. The primary concern is achieving a sufficiently strong electron-photon coupling $|g_q| \sim 1$ for effective quantum state reconstruction (SM). While recent experiments have approached this threshold [51], issues with losses and decoherence of the electron wave function persist [89]. Specifically, the interaction between electrons and photons must be much stronger than other channels of electron energy losses. Another challenge for FEQOD in the optical domain relates to electron beam conditions for grazing interaction, necessitating a narrow, collimated beam maintaining a constant distance from the photonic structure to minimize fluctuations in g_q [38]. For implementing FEQOD in the infrared domain, a narrower electron energy spread is also needed. Current ultrafast electron microscopes typically have an energy spread around 1 eV [35,38–46,50,52–56,61,62], which can be reduced using electron monochromators [90,91]. Ongoing advancements in electron microscopy pave the way for higher-quality FEQOD implementations. Future developments of such capabilities in free-electron quantum optics could have an impact on studies at the foundations of quantum mechanics, from quantum tomography [18–20] to weak measurements [92].

Acknowledgments—This research is funded in part by the Gordon and Betty Moore Foundation, through Grant No. GBMF11473 to I. K. It is also partially supported under the Flagship research project QUBIT by the Helen Diller Quantum Center at the Technion and the Israel Science Foundation (ISF), Grant No. 385/23. A. G. gratefully acknowledge the support of Azrieli Scholarship. E. C was supported by the Israel Science Foundation (Grant No. 2208/24).

[1] L. Mandel and E. Wolf, *Optical Coherence and Quantum Optics* (Cambridge University Press, Cambridge, 1995).
[2] M. O. Scully and Z. M. S., *Quantum Optics* (Cambridge University Press, Cambridge, 1997).
[3] C. Gerry, P. Knight, and P. L. Knight, *Introductory Quantum Optics* (Cambridge University Press, Cambridge, 2005).
[4] J. Garrison and R. Chiao, *Quantum Optics* (Oxford University Press, Oxford, 2008).
[5] A. Aspect, J. Dalibard, and G. Roger, Experimental test of Bell's inequalities using time-varying analyzers, Phys. Rev. Lett. **49**, 1804 (1982).
[6] C. K. Hong, Z. Y. Ou, and L. Mandel, Measurement of subpicosecond time intervals between two photons by interference, Phys. Rev. Lett. **59**, 2044 (1987).
[7] P. Grangier, G. Roger, and A. Aspect, Experimental evidence for a photon anticorrelation effect on a beam splitter: A new light on single-photon interferences, Europhys. Lett. **1**, 173 (1986).
[8] D. T. Smithey, M. Beck, M. G. Raymer, and A. Faridani, Measurement of the Wigner distribution and the density matrix of a light mode using optical homodyne tomography: Application to squeezed states and the vacuum, Phys. Rev. Lett. **70**, 1244 (1993).
[9] G. Breitenbach, S. Schiller, and J. Mlynek, Measurement of the quantum states of squeezed light, Nature (London) **387**, 471 (1997).
[10] P. Kok, W. J. Munro, K. Nemoto, T. C. Ralph, J. P. Dowling, and G. J. Milburn, Linear optical quantum computing with photonic qubits, Rev. Mod. Phys. **79**, 135 (2007).
[11] A. Politi, J. C. F. Matthews, and J. L. O'Brien, Shor's quantum factoring algorithm on a photonic chip, Science **325**, 1221 (2009).
[12] J. Aasi *et al.*, Enhanced sensitivity of the LIGO gravitational wave detector by using squeezed states of light, Nat. Photonics **7**, 613 (2013).
[13] A. Boaron *et al.*, Secure quantum key distribution over 421 km of optical fiber, Phys. Rev. Lett. **121**, 190502 (2018).
[14] H.-S. Zhong *et al.*, Quantum computational advantage using photons, Science **370**, 1460 (2020).
[15] R. H. Brown and R. Q. Twiss, Correlation between photons in two coherent beams of light, Nature (London) **177**, 27 (1956).
[16] L. A. Jiang, E. A. Dauler, and J. T. Chang, Photon-number-resolving detector with 10 bits of resolution, Phys. Rev. A **75**, 062325 (2007).
[17] A. Divochiy *et al.*, Superconducting nanowire photon-number-resolving detector at telecommunication wavelengths, Nat. Photonics **2**, 302 (2008).
[18] U. Leonhardt, *Measuring the Quantum State of Light* (Cambridge University Press, Cambridge, 1997), Vol. 22.
[19] A. I. Lvovsky and M. G. Raymer, Continuous-variable optical quantum-state tomography, Rev. Mod. Phys. **81**, 299 (2009).
[20] R. Nehra, A. Win, M. Eaton, R. Shahrokhshahi, N. Sridhar, T. Gerrits, A. Lita, S. W. Nam, and O. Pfister, State-independent quantum state tomography by photon-number-resolving measurements, Optica **6**, 1356 (2019).
[21] S. Cova, M. Ghioni, A. Lacaita, C. Samori, and F. Zappa, Avalanche photodiodes and quenching circuits for single-photon detection, Appl. Opt. **35**, 1956 (1996).

[22] S. Pellegrini, R. E. Warburton, L. J. J. Tan, J. S. Ng, A. B. Krysa, K. Groom, J. P. R. David, S. Cova, M. J. Robertson, and G. S. Buller, Design and performance of an InGaAs-InP single-photon avalanche diode detector, IEEE J. Quantum Electron. **42**, 397 (2006).
[23] F. Ceccarelli, G. Acconcia, A. Gulinatti, M. Ghioni, I. Rech, and R. Osellame, Recent advances and future perspectives of single-photon avalanche diodes for quantum photonics applications, Adv. Quantum Technol. **4**, 2000102 (2021).
[24] C. M. Natarajan, M. G. Tanner, and R. H. Hadfield, Superconducting nanowire single-photon detectors: physics and applications, Supercond. Sci. Technol. **25**, 063001 (2012).
[25] B. G. Oripov, D. S. Rampini, J. Allmaras, M. D. Shaw, S. W. Nam, B. Korzh, and A. N. McCaughan, A superconducting nanowire single-photon camera with 400,000 pixels, Nature (London) **622**, 730 (2023).
[26] W. Becker, *Advanced Time-Correlated Single Photon Counting Techniques* (Springer, Berlin Heidelberg, 2005), Vol. 81.
[27] D. Renker and E. Lorenz, Advances in solid state photon detectors, J. Instrum. **4**, P04004 (2009).
[28] P. Goy, J. M. Raimond, M. Gross, and S. Haroche, Observation of cavity-enhanced single-atom spontaneous emission, Phys. Rev. Lett. **50**, 1903 (1983).
[29] A. M. Herkommer, V. M. Akulin, and W. P. Schleich, Quantum demolition measurement of photon statistics by atomic beam deflection, Phys. Rev. Lett. **69**, 3298 (1992).
[30] J. M. Raimond, M. Brune, and S. Haroche, Colloquium: Manipulating quantum entanglement with atoms and photons in a cavity, Rev. Mod. Phys. **73**, 565 (2001).
[31] S. Deleglise, I. Dotsenko, C. Sayrin, J. Bernu, M. Brune, J.-M. Raimond, and S. Haroche, Reconstruction of nonclassical cavity field states with snapshots of their decoherence, Nature (London) **455**, 510 (2008).
[32] C. Flühmann and J. P. Home, Direct characteristic-function tomography of quantum states of the trapped-ion motional oscillator, Phys. Rev. Lett. **125**, 043602 (2020).
[33] Y. Shaked, Y. Michael, R. Z. Vered, L. Bello, M. Rosenbluh, and A. Pe'er, Lifting the bandwidth limit of optical homodyne measurement with broadband parametric amplification, Nat. Commun. **9**, 609 (2018).
[34] G. Frascella, E. E. Mikhailov, N. Takanashi, R. V Zakharov, O. V Tikhonova, and M. V Chekhova, Wide-field SU(1,1) interferometer, Optica **6**, 1233 (2019).
[35] B. Barwick, D. J. Flannigan, and A. H. Zewail, Photon-induced near-field electron microscopy, Nature (London) **462**, 902 (2009).
[36] O. Kfir, Entanglements of electrons and cavity photons in the strong-coupling regime, Phys. Rev. Lett. **123**, 103602 (2019).
[37] V. Di Giulio, M. Kociak, and F. J. G. de Abajo, Probing quantum optical excitations with fast electrons, Optica **6**, 1524 (2019).
[38] R. Dahan *et al.*, Resonant phase-matching between a light wave and a free-electron wavefunction, Nat. Phys. **16**, 1123 (2020).
[39] A. Feist, K. E. Echternkamp, J. Schauss, S. V Yalunin, S. Schäfer, and C. Ropers, Quantum coherent optical phase modulation in an ultrafast transmission electron microscope, Nature (London) **521**, 200 (2015).
[40] K. Wang, R. Dahan, M. Shentcis, Y. Kauffmann, A. Ben Hayun, O. Reinhardt, S. Tsesses, and I. Kaminer, Coherent interaction between free electrons and a photonic cavity, Nature (London) **582**, 50 (2020).
[41] O. Kfir, H. Lourenço-Martins, G. Storeck, M. Sivis, T. R. Harvey, T. J. Kippenberg, A. Feist, and C. Ropers, Controlling free electrons with optical whispering-gallery modes, Nature (London) **582**, 46 (2020).
[42] Y. Adiv *et al.*, Quantum nature of dielectric laser accelerators, Phys. Rev. X **11**, 041042 (2021).
[43] J.-W. Henke *et al.*, Integrated photonics enables continuous-beam electron phase modulation, Nature (London) **600**, 653 (2021).
[44] A. Feist *et al.*, Cavity-mediated electron-photon pairs, Science **377**, 777 (2022).
[45] G. Huang, N. J. Engelsen, O. Kfir, C. Ropers, and T. J. Kippenberg, Electron-photon quantum state heralding using photonic integrated circuits, PRX Quantum **4**, 020351 (2023).
[46] K. E. Priebe, C. Rathje, S. V Yalunin, T. Hohage, A. Feist, S. Schäfer, and C. Ropers, Attosecond electron pulse trains and quantum state reconstruction in ultrafast transmission electron microscopy, Nat. Photonics **11**, 793 (2017).
[47] Z. Xie, Z. Chen, H. Li, Q. Yan, H. Chen, X. Lin, I. Kaminer, O. D. Miller, and Y. Yang, Maximal quantum interaction between free electrons and photons, arXiv:2404.00377.
[48] Z. Zhao, Upper bound for the quantum coupling between free electrons and photons, arXiv:2404.01221.
[49] V. Di Giulio, E. Akerboom, A. Polman, and F. J. García de Abajo, Toward optimum coupling between free electrons and confined optical modes, ACS Nano **18**, 14255 (2024).
[50] A. Karnieli, C. Roques-Carmes, N. Rivera, and S. Fan, Strong coupling and single-photon nonlinearity in free-electron quantum optics, ACS Photonics (2024).
[51] Y. Adiv, H. Hu, S. Tsesses, R. Dahan, K. Wang, Y. Kurman, A. Gorlach, H. Chen, X. Lin, and G. Bartal, Observation of 2D Cherenkov radiation, Phys. Rev. X **13**, 011002 (2023).
[52] D. Nabben, J. Kuttruff, L. Stolz, A. Ryabov, and P. Baum, Attosecond electron microscopy of sub-cycle optical dynamics, Nature (London) **619**, 63 (2023).
[53] J. H. Gaida, H. Lourenço-Martins, M. Sivis, T. Rittmann, A. Feist, F. J. García de Abajo, and C. Ropers, Attosecond electron microscopy by free-electron homodyne detection, Nat. Photonics **18**, 509 (2024).
[54] T. Bucher, H. Nahari, H. H. Sheinfux, R. Ruimy, A. Niedermayr, R. Dahan, Q. Yan, Y. Adiv, M. Yannai, and J. Chen, Coherently amplified ultrafast imaging in a free-electron interferometer, Nat. Photonics **18**, 809 (2024).
[55] R. Dahan *et al.*, Imprinting the quantum statistics of photons on free electrons, Science **373**, 6561 (2021).
[56] Y. Yang, J.-W. Henke, A. S. Raja, F. J. Kappert, G. Huang, G. Arend, Z. Qiu, A. Feist, R. N. Wang, and A. Tusnin, Free-electron interaction with nonlinear optical states in microresonators, Science **383**, 168 (2024).
[57] R. T. Menzies, Laser heterodyne detection techniques, in *Laser Monitoring of the Atmosphere* (Springer-Verlag, Berlin Heidelberg, 2005), p. 297.

[58] S. M. Gallagher, A. W. Albrecht, J. D. Hybl, B. L. Landin, B. Rajaram, and D. M. Jonas, Heterodyne detection of the complete electric field of femtosecond four-wave mixing signals, J. Opt. Soc. Am. B **15**, 2338 (1998).
[59] X. Zhang, Q.-T. Cao, Z. Wang, Y. Liu, C.-W. Qiu, L. Yang, Q. Gong, and Y.-F. Xiao, Symmetry-breaking-induced nonlinear optics at a microcavity surface, Nat. Photonics **13**, 21 (2019).
[60] R. Nehra, R. Sekine, L. Ledezma, Q. Guo, R. M. Gray, A. Roy, and A. Marandi, Few-cycle vacuum squeezing in nanophotonics, Science **377**, 1333 (2022).
[61] S. T. Park, M. Lin, and A. H. Zewail, Photon-induced near-field electron microscopy (PINEM): Theoretical and experimental, New J. Phys. **12**, 123028 (2010).
[62] F. J. G. De Abajo, Optical excitations in electron microscopy, Rev. Mod. Phys. **82**, 209 (2010).
[63] S. V Yalunin, A. Feist, and C. Ropers, Tailored high-contrast attosecond electron pulses for coherent excitation and scattering, Phys. Rev. Res. **3**, L032036 (2021).
[64] See Supplemental Material at http://link.aps.org/supplemental/10.1103/PhysRevLett.133.250801 for the derivation of the equations from the main text. It also clarifies some aspects of applicability of the suggested method of free-electron quantum optical detection.
[65] G. Arend *et al.*, Electrons herald non-classical light, arXiv:2409.11300.
[66] Z. Zhao, Upper bound for the quantum coupling between free electrons and photons, arXiv:2404.01221.
[67] R. H. Hadfield, Single-photon detectors for optical quantum information applications, Nat. Photonics **3**, 696 (2009).
[68] Y. Morimoto and P. Baum, Diffraction and microscopy with attosecond electron pulse trains, Nat. Phys. **14**, 252 (2018).
[69] M. Kozák, N. Schönenberger, and P. Hommelhoff, Ponderomotive generation and detection of attosecond free-electron pulse trains, Phys. Rev. Lett. **120**, 103203 (2018).
[70] G. M. Vanacore *et al.*, Attosecond coherent control of free-electron wave functions using semi-infinite light fields, Nat. Commun. **9**, 2694 (2018).
[71] A. Ben Hayun, O. Reinhardt, J. Nemirovsky, A. Karnieli, N. Rivera, and I. Kaminer, Shaping quantum photonic states using free electrons, Sci. Adv. **7**, 4270 (2021).
[72] R. Dahan, G. Baranes, A. Gorlach, R. Ruimy, N. Rivera, and I. Kaminer, Creation of optical cat and GKP states using shaped free electrons, Phys. Rev. X **13**, 031001 (2023).
[73] G. Baranes, S. Even-Haim, R. Ruimy, A. Gorlach, R. Dahan, A. A. Diringer, S. Hacohen-Gourgy, and I. Kaminer, Free-electron interactions with photonic GKP states: Universal control and quantum error correction, Phys. Rev. Res. **5**, 043271 (2023).
[74] A. Karnieli and S. Fan, Jaynes-Cummings interaction between low-energy free electrons and cavity photons, Sci. Adv. **9**, eadh2425 (2023).
[75] V. Di Giulio and F. J. García de Abajo, Optical-cavity mode squeezing by free electrons, Nanophotonics **11**, 4659 (2022).
[76] A. Karnieli, S. Tsesses, R. Yu, N. Rivera, A. Arie, I. Kaminer, and S. Fan, Universal and ultrafast quantum computation based on free-electron-polariton blockade, PRX Quantum **5**, 010339 (2024).
[77] S. Hacohen-Gourgy, L. S. Martin, E. Flurin, V. V Ramasesh, K. B. Whaley, and I. Siddiqi, Quantum dynamics of simultaneously measured non-commuting observables, Nature (London) **538**, 491 (2016).
[78] P. Reinhold, S. Rosenblum, W.-L. Ma, L. Frunzio, L. Jiang, and R. J. Schoelkopf, Error-corrected gates on an encoded qubit, Nat. Phys. **16**, 822 (2020).
[79] S. Rosenblum, P. Reinhold, M. Mirrahimi, L. Jiang, L. Frunzio, and R. J. Schoelkopf, Fault-tolerant detection of a quantum error, Science **361**, 266 (2018).
[80] A. Polman, M. Kociak, and F. J. García de Abajo, Electron-beam spectroscopy for nanophotonics, Nat. Mater. **18**, 1158 (2019).
[81] M. Kjaergaard, M. E. Schwartz, J. Braumüller, P. Krantz, J. I.-J. Wang, S. Gustavsson, and W. D. Oliver, Superconducting qubits: Current state of play, Annu. Rev. Condens. Matter Phys. **11**, 369 (2020).
[82] L. Henriet, L. Beguin, A. Signoles, T. Lahaye, A. Browaeys, G.-O. Reymond, and C. Jurczak, Quantum computing with neutral atoms, Quantum **4**, 327 (2020).
[83] A. Gover and A. Yariv, Free-electron-bound-electron resonant interaction, Phys. Rev. Lett. **124**, 064801 (2020).
[84] Z. Zhao, X.-Q. Sun, and S. Fan, Quantum entanglement and modulation enhancement of free-electron–bound-electron interaction, Phys. Rev. Lett. **126**, 233402 (2021).
[85] R. Ruimy, A. Gorlach, C. Mechel, N. Rivera, and I. Kaminer, Toward atomic-resolution quantum measurements with coherently shaped free electrons, Phys. Rev. Lett. **126**, 233403 (2021).
[86] F. J. García de Abajo and V. Di Giulio, Optical excitations with electron beams: Challenges and opportunities, ACS Photonics **8**, 945 (2021).
[87] A. Gorlach, O. Reinhardt, A. Pizzi, R. Ruimy, G. Baranes, N. Rivera, and I. Kaminer, Double-superradiant cathodoluminescence, Phys. Rev. A **109**, 023722 (2024).
[88] A. Karnieli, S. Tsesses, R. Yu, N. Rivera, Z. Zhao, A. Arie, S. Fan, and I. Kaminer, Quantum sensing of strongly coupled light-matter systems using free electrons, Sci. Adv. **9**, eadd2349 (2023).
[89] M. Tsarev, A. Ryabov, and P. Baum, Measurement of temporal coherence of free electrons by time-domain electron interferometry, Phys. Rev. Lett. **127**, 165501 (2021).
[90] K. Kimoto, Practical aspects of monochromators developed for transmission electron microscopy, J. Electron Microsc. **63**, 337 (2014).
[91] M. Yannai, Y. Adiv, R. Dahan, K. Wang, A. Gorlach, N. Rivera, T. Fishman, M. Krüger, and I. Kaminer, Lossless monochromator in an ultrafast electron microscope using near-field THz radiation, Phys. Rev. Lett. **131**, 145002 (2023).
[92] B. Tamir and E. Cohen, Introduction to weak measurements and weak values, Quanta **2**, 7 (2013).